CFD with OpenSource software

A course at Chalmers University of Technology
Taught by Håkan Nilsson

Study questions and answers for:

Project work:

Implementation of Elliptic Blending Reynolds Stress Model in OpenFoam

---

Author:
Ardalan Javadi

Peer reviewed by:
Håkan Nilsson

March 5, 2016

1 Introduction

Modeling the effects of solid walls on adjacent turbulent flows has long been—and still is—a major challenge. The problem is equally acute in one-point and two-point statistical closures, as it is in spectral modeling or large-eddy simulations (LES). Indeed, the hypotheses underlying existing one-point turbulence closure models, e.g., high Reynolds number, local isotropy, quasi-homogeneity, are not valid in the presence of a wall. Hence, near-wall modifications are necessary in order to make them comply with the near-wall behavior of turbulence.

In this contribution, Elliptic Blending Reynolds stress model (EBRSM) proposed by Manceau and Hanjalić [7] is implemented and verified in various flow fields. To blend the consistency and accuracy for industrial applications and simplicity of the model, EBRSM follows the elliptic blending model of Durbin [1]. Durbin's model enables the integration down to the wall, with acceptable grid density. The method, applied to Reynolds stress models, has a solid theoretical basis, but implies six additional equations, which impedes its spreading into the industry. The main problem is not the increased cost due to the number of equations, but rather the complexity of the implementation and the stability problems: the boundary conditions for the additional equations are a major source of numerical instability. The EBRSM reduces the number of equations in Durbin's Reynolds stress model and thus to reduce the complexity of the model.

1.1 The physics of wall effects on turbulence

A solid wall exerts multiple effects on fluid flow and turbulence. There are two fundamental mechanisms by which a solid boundary affects turbulence : (i) generation of a mean velocity gradient (via the no-slip condition) which, upon interaction with turbulent shear stress, supplies energy to turbulence ; and (ii) suppression (or blocking) of velocity fluctuations in its vicinity. The first effect can be regarded as dynamical and the second effect may be viewed as primarily kinematic. Here, it is hypothesized that the two effects are separate in affecting flow dynamics.

There is evidence that both the hairpins and streaks may be due to the effect of shear rate rather than due to the suppression of turbulence by the wall. For example, Uzkan and Reynolds [2] conducted a shear-free turbulent boundary-layer experiment by passing grid-generated turbulence over a moving wall. When the speed of the moving wall was matched to that of the free stream, a shear-free boundary layer was produced and the near-wall streaks disappeared in the absence of mean shear. A related experiment was performed by Thomas and Hancock [3] at a higher Reynolds number. Rogers and Moin [4], using direct numerical simulation of a homogeneous shear flow, found the presence of hairpin vortices similar to those observed in the logarithmic layer of wall-bounded turbulent flows. However, their computed velocity patterns did not reveal elongated streaky structures; in fact, the shear rate in their computation was comparable with that in the logarithmic layer of a turbulent boundary layer. It should be noted that in a homogeneous turbulent flow there is no solid boundary to suppress velocity fluctuations.

The effect of blocking velocity fluctuations near a surface leads to a net transfer of energy from the vertical component of turbulence to the horizontal components [5]. This redistribution effect appears to be the reason why the vertical component of the pressure-strain-rate term, $\overline{p\partial v/\partial y}$, changes sign in the vicinity of the surface [6]. However, the effect of the boundary is not important for small eddies at $y \geq L$, where L is the integral length scale. A physically consistent model ought to account separately for each of the effects mentioned, something that is difficult to achieve with a limited number of flow and turbulence parameters that are at one's disposal in one-point turbulence models, regardless of their level. Thus, the behavior of the flow should be taken into account in correct modelling of the wall effects.

Most models of near-wall turbulence do not distinguish the viscous from nonviscous effects and usually apply empirical damping functions in terms of local turbulence Reynolds numbers and often of wall distance by which to account for the total wall effect. Needless to say, such models cannot perform well in situations where one or the other effect is absent or is of less importance (e.g., viscous and transitional regions in flows away from a solid wall unaffected by blocking, or flows with liquid–gas interface where the kinematic blocking is the sole cause of turbulence modification). A better approach should considered to account for both effects.

1.2 Rationale of Elliptic Blending Model

The elliptic blending model reduces the number of equations in Durbin's Rey-nolds stress model and thus the complexity of the model. Durbin's model with six elliptic differential equations with boundary conditions enables the reproduction of the near-wall behavior of the redistribution term. These equations have then

the purely geometrical effect, with a unique length scale, L. Their role is to enforce the redistribution terms to comply with their near-wall limiting behavior. It is, therefore, expected that the same effect could be reproduced with only one elliptic equation, $\alpha - \nabla^2\alpha = 1/k$, where α is elliptic function and k is the turbulent kinetic energy.

The Reynolds stresses behave as y^2 , if y represents the direction normal to a wall located in y=0 (as shown below, the behaviour in y^n , with $n > 2$, of some components is due to the blockage effect). The boundary condition $u_i u_j = 0$ is not sufficient to impose this behaviour, which requires the correct reproduction of the balance between viscous diffusion and dissipation in the Reynolds stress transport equations in the vicinity of the wall. This requirement is consequently linked to the correct modelling of the dissipation tensor: since the viscous damping also suppresses the scale separation between energetic and dissipative structures, the anisotropy of the dissipation tensor cannot be neglected. In practice, the correct asymptotic behaviour is obtained in near-wall Reynolds-stress models by choosing a model for the dissipation tensor that satisfies

$$\lim_{y\to 0} \epsilon_{ij} = 2\nu \lim_{y\to 0} \frac{\overline{u_i u_j}}{y2}. \tag{1}$$

The implementation of the model is done with OpenFOAM-2.3x and started from LRR model available in the code. Since the dicrepencies between LRR and EBRSM is remarkable, the original LRR should be modified. In this context, the following steps should be done in LRR.C file.

- Remove all constant coefficients, e.g. lines 58-132.
- Introduce the appropriate constant coefficients of EBRSM mentioned at the end of section 3.
- Remove `couplingFactor_`, e.g. lines 267-289 and lines 313-321.
- Remove ϵ and R equations, e.g. lines 348-420.
- Remove functions to correct the wall shear stresses, e.g. the lines 423-465.

Introduce the corresponding functions in LRR.H. Rename the files LRR.C and LRR.H to EBRSM.C and EBRSM.H, respectivly, and recompile it.

The implementation of the boundary condition for ϵ in the code is

```
forAll(mesh_.boundary(),i)}
{
if(mesh_.boundary()[i].type()=="wall")
    {
    scalarField & refepsilonboundary = epsilon_.boundaryField()[i];
    scalarField knearwall  = k_.boundaryField()[i].patchInternalField();

        epsilon_.boundaryField()[i].patchInternalField()=
            2.0/nearWallDist(mesh_).y()[i]/nearWallDist(mesh_).y()[i]
            *nu()*mag(knearwall);
    }
}
```

where these lines should be copied after the production term in EBRSM.C code.

For a free-slip surface, components $\overline{u^2}$ and $\overline{w^2}$ behave as y^0 and $\overline{v^2}$ as y^2; for a no-slip surface, this asymptotic behaviour is changed to y^2 and y^4, respectively. In all cases, the most important effect to take into account is the fact that $\overline{v^2}$ is negligible compared to the other normal stresses, such that turbulence reaches a *two-component* limit in the vicinity of the surface. In the case of a no-slip wall, one of the main difficulties lies in the particular scales of this phenomenon, linked to the non-locality of the fluctuating pressure, at the origin of a sensitivity of turbulence to the blockage effect up to a distance to the wall much larger than the thickness of the viscous sublayer. In order to model this blockage effect, the correct reproduction of the near-wall balance between viscous diffusion and dissipation, Eq. 1, is not sufficient: the asymptotic behaviour of the velocity-pressure gradient correlation term must be accounted for. This is the main purpose of the Elliptic Blending method.

The presence of a wall induces an increase of pressure fluctuations, called the *wall-echo* effect. In RANS modelling, the wall echo effect specifically denotes the consequence of the existence of this echo for the velocity-pressure gradient correlation involved in the Reynolds stress transport equations. The wall blockage and the wall echo are always coupled. In terms of modelling, it is important to remark that the two

effects have opposite influences on pressure-strain term in most of the near-wall region, in particular for its redistributive part.

The main objective of Elliptic Relaxation and Elliptic Blending approaches is to account for the influence of the wall blockage on the energy redistribution towards the wall-normal component, which is necessary to reproduce the two-component limit of turbulence.

2 The Elliptic Blending Approach

Equation 2 shows the pressure-strain term in the EBRSM,

$$\phi_{ij} = (1-\alpha^3)\phi^w_{ij} + \alpha^3\phi^h_{ij}, \tag{2}$$

where ϕ^h_{ij} is a standard model of the rapid part in the pressure-strain term. The main feature of Elliptic Blending, the reproduction of the blockage effect, is due to the fact that the elliptic operator ensures a smooth relaxation from the correct asymptotic behaviour of ϕ_{ij}, pressure-strain term, imposed by the boundary conditions to the standard model ϕ^h_{ij}, see Eq. 2. Manceau and Hanjalić [7] proposed the Elliptic Blending approach, for the purpose of building a model preserving the desirable features of Elliptic relaxation.

The method consists in ensuring the transition from the near wall to the weakly inhomogeneous behaviour using a single scalar function, α in Eq. 2, which must tend to 0 at the wall and to 1 far from the wall, under the form

The near-wall form of the pressure-strain term is ϕ^w_{ij}. The function α reads

$$\alpha - L^2\nabla^2\alpha = 1. \tag{3}$$

The implementation in the code (copy these lines after the production term in the code and before boundary condition for ϵ) is

```
tmp<fvScalarMatrix> alphaEqn
    (
    fvm::Sp(OneoverL2,alpha_)
   -fvm::laplacian(One,alpha_)
        ==
        OneoverL2
    );
    alphaEqn().relax();
    solve(alphaEqn);
```

where `OneoverL2` is

```
volScalarField OneoverL2 =1./(L*L);
```

with the boundary condition $\alpha = 0$ at the wall. The solution of this equation goes to zero at the wall and to one far from the wall, thus providing the appropriate blending between the two formulations ϕ^h_{ij} and ϕ^w_{ij}. The thickness of the region of influence of the near-wall model is driven by the length scale L,

$$L = C_L max\left(\frac{k^{3/2}}{\epsilon}, C_\eta\frac{\nu^{3/4}}{\epsilon^{1/4}}\right), \tag{4}$$

which is implemented in the code as

```
volScalarField L = CL * max(pow(k_,1.5)/epsilon_,
                  Ceta * pow(nu(), 0.75)/pow(epsilon_,0.25));
```

where these lines should be copied before the production term in the code.

The term ϕ^h_{ij} in Eq. 2 reads

$$\begin{aligned}\phi^h_{ij} = -\left(g_1 + g^*_1\frac{P}{\epsilon}\right)\epsilon a_{ij} + g_2\epsilon\left(a_{ik}a_{kj} - \frac{1}{3}a_{kl}a_{kl}\delta_{ij}\right)\\ + \left(g_3 - g^*_3\sqrt{a_{kl}a_{kl}}\right)kS_{ij}\\ + g_4k\left(a_{ik}S_{jk} + a_{jk}S_{ik} - \frac{2}{3}a_{lm}S_{lm}\delta_{ij}\right)\\ + g_5k\left(a_{ik}W_{jk} + a_{jk}W_{ik}\right),\end{aligned} \tag{5}$$

where $a_{ij} = \overline{u_i u_j}/2k - \delta_{ij}/3$ is the anisotropy tensor, S_{ij} is the strain rate tensor and W_{ij} is the vorticity tensor, P is the the trace of production tensor.

Note that in this version of the model $g_2 = 0$. Now, the model is not very sensitive to a coarsening of the near-wall mesh, as long as the first point is located in the viscous sublayer ($y^+ < 5$). To introduce ϕ^h_{ij}, the strain and vorticity rates are needed. They are implemented as

```
volTensorField    gradU =  fvc::grad(U_);
volTensorField    S = 0.5*((gradU.T()+gradU));
volSymmTensorField Ssym = symm(S);
volTensorField    W = 0.5*((gradU.T()-gradU));
```

where these lines should be copied before the production term in the code.

```
volSymmTensorField a = dev(R_)/tr(R_);

volSymmTensorField isotrope =
        1.0/3.0*alpha_*alpha_*alpha_*(g1*epsilon_ + g1star*G)*I;

volScalarField anisotrope =
        alpha_*alpha_*alpha_*(g1*epsilon_ + g1star*G)/2.0/k_;

volSymmTensorField phih =
        k_*symm(S*(g3-g3star*sqrt(b&&b)))
        +g4*k_*(twoSymm(b & S) - 2.0/3.0*I* (b && S) )
        +g5*k_*twoSymm(b & W.T());
```

where these lines should be copied after boundary condition for ϵ and then do the following.

The term ϕ^w_{ij} in Eq. 2 reads

$$\phi^w_{ij} = -5\frac{\epsilon}{k}\left(\overline{u_i u_k}n_j n_k + \overline{u_j u_k}n_i n_k - \frac{1}{2}\overline{u_i u_k}n_k n_l n_j n_j - \frac{1}{2}\overline{u_k u_l}n_k n_l \delta_{ij}\right), \tag{6}$$

where n is wall normal vector which reads

$$n = \frac{\nabla\alpha}{\|\nabla\alpha\|} \tag{7}$$

where the implementation of $\nabla\alpha$ and n is

```
volVectorField gradalpha = fvc::grad(alpha_);
volVectorField n = gradalpha/mag(gradalpha);
```

Different terms of ϕ^w_{ij} and ϕ_{ij} are implemented as

```
volVectorField Rn = R_&n;
volTensorField Rnn = Rn*n;

 volSymmTensorField phiw = -5.0*epsilon_/k_*
    symm(
    (Rnn + Rnn.T() -0.5*((R_ & n & n)* (n*n + I)))
    );

volSymmTensorField phi =
       (One - alpha_*alpha_*alpha_)* phiw
       + alpha_*alpha_*alpha_*phih;
```

where these lines should be copied after the boundary condition for ϵ.

3 Elliptic Blending Reynolds-stress Model

The Reynolds-stress transport equation reads

$$\frac{D\overline{u_i u_j}}{Dt} = P_{ij} + D^{\nu}_{ij} + D^{T}_{ij} + \phi_{ij} - \epsilon_{ij}, \tag{8}$$

where P_{ij}, D^{ν}_{ij}, D^{T}_{ij}, ϕ_{ij} and ϵ_{ij} stands for the production, the molecular diffusion, the turbulent diffusion, the pressure-strain correlation and the dissipation tensor, respectively. The implementation of the pressure-strain term is discussed in section 2. The implementation of the other terms are discussed in this section. The turbulent diffusion is given by

$$D^{T}_{ij} = \frac{\partial}{\partial x_l}\left(\frac{C_\mu}{\sigma_k}\overline{u_l u_m} T \frac{\partial \overline{u_i u_j}}{\partial x_m}\right). \tag{9}$$

This term is implemented in the Reynolds-stresses equation at the end of this section.
The dissipation tensor is given by

$$\epsilon_{ij} = \left(1-\alpha^3\right)\frac{\overline{u_i u_j}}{k}\epsilon + \frac{2}{3}\alpha^3 \epsilon \delta_{ij}. \tag{10}$$

The implementation of the dissipation tensor is done as

```
volScalarField epsilonterm1 =
       (One- alpha_*alpha_*alpha_)*epsilon_/k_;
volSymmTensorField epsilonterm2 =
       2.0/3.0 * I* alpha_*alpha_*alpha_*epsilon_
       + 0.0*((One- alpha_*alpha_*alpha_)*epsilon_/k_)*R_;
```

where, `One` is a scalar 1 and `epsilon_` is calculated from the dissipation equation in the following. These lines should be copied after the pressure-strain terms.
Time scale is given by

$$T = max\left(\frac{k}{\epsilon}, C_T\left(\frac{\nu}{\epsilon}\right)^{1/2}\right), \tag{11}$$

which is implemented as

```
volScalarField TEBM = max(k_/epsilon_, CT * sqrt(nu()/epsilon_));
```

where these lines should be copied after length scale, L, in the code.

The dissipation equation is given by

$$\frac{D\epsilon}{Dt} = \frac{C^{'}_{\epsilon 1}P - C_{\epsilon 2}\epsilon}{T} + \frac{\partial}{\partial x_l}\left(\frac{C_\mu}{\sigma_\epsilon}\overline{u_l u_m} T \frac{\partial \epsilon}{\partial x_m}\right) + \nu \frac{\partial^2 \epsilon}{\partial x_k \partial x_k} \tag{12}$$

$$C^{'}_{\epsilon 1} = C_{\epsilon 1}\left[1 + A_1(1-\alpha^3)\frac{P}{\epsilon}\right] \tag{13}$$

where, $C^{'}_{\epsilon 1}$ given by Eq. 13 is implemented as

```
volScalarField Cepsilon1bar =
           Cepsilon1* (1.0 + A1*(One-alpha_*alpha_*alpha_)
           *(G/epsilon_));.
```

where these lines should be copied after the production term.

The dissipation equation, Eq. 12, is implemented as

```
tmp<fvScalarMatrix> epsEqn
(
    fvm::ddt(epsilon_)
  + fvm::div(phi_, epsilon_)
  - fvm::Sp(fvc::div(phi_), epsilon_)
  - fvm::laplacian(CMu/sigmaepsilon*R_*TEBM, epsilon_)
```

```
    - fvm::laplacian(nu(), epsilon_)
      ==
    - fvm::Sp(Cepsilon2/TEBM, epsilon_)
    + Cepsilon1bar*G/TEBM
  );
  epsEqn().relax();
  solve(epsEqn); .
```

where the two laplacian terms on the right-hand side are turbulent and viscous diffusion, respectively. These lines should be copied after the boundary condition for ϵ.

The implementation of the Reynolds-stress equation, Eq. 8, is done as

```
tmp<fvSymmTensorMatrix> REqn
(
    fvm::ddt(R_)
    + fvm::div(phi_, R_)
    - fvm::Sp(fvc::div(phi_), R_)
    - fvm::laplacian(nu(), R_)
    - fvm::laplacian(CMu/sigmak*TEBM*R_,R_)
    + fvm::Sp(anisotrope, R_)
    + fvm::Sp(epsilonterm1, R_)

  ==

    P
    + isotrope
    - epsilonterm2
    + phistar
);
REqn().relax();
solve(REqn);
```

where these lines should be copied after `epsilonterm2` in the code.

The coefficients are given by
$g_1 = 3.4$, $g_1^* = 1.8$, $g_3 = 0.8$, $g_3^* = 1.3$, $g_4 = 1.25$, $g_5 = 0.4$,
$C_\mu = 0.21$, $\sigma_k = 1.0$, $C_T = 6.0$, $C_L = 0.133$, $C_\eta = 80.0$, $C_\epsilon 1 = 1.44$,
$C_\epsilon 2 = 1.83$, $A_1 = 0.065$, $\sigma_\epsilon = 1.15$.

4 Validation of the Implementation

The implementation is validated with four test cases

- channel flow with $Re_\tau = 590$
- periodic hill with $Re = 10595$
- a symmetric diffuser with $Re = 18000$
- Dellenback abrupt expansion with $Re = 100000$, $Sr = 1.23$.

The calculations reported herein are made using the finite-volume method in the OpenFOAM-2.3x CFD code. The second-order central differencing scheme is used to discretize the diffusion terms. The linear-upwind differencing is used to approximate the convection term. Time marching is performed with an implicit second-order accurate backward differentiation scheme. The solver used in all simulations is *pisoFoam*.

4.1 Channel Flow

The Reynolds number based on the wall stress is $Re_\tau = 595$. Periodic boundary conditions are applied in the streamwise direction. The mesh is $N_x \times N_y = 80 \times 5$. The pressure gradient that drives the flow is adjusted dynamically to maintain a constant mass flux through the channel. The results are compared with the DNS of Moser et al. [9], see Fig. 1.

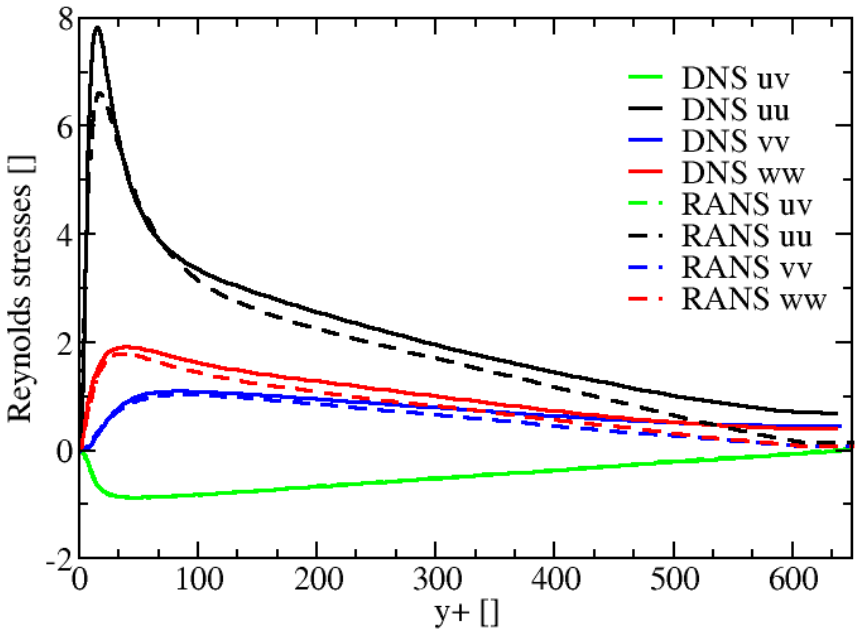

Figure 1: Reynolds stresses in the channel, $Re_\tau = 590$.

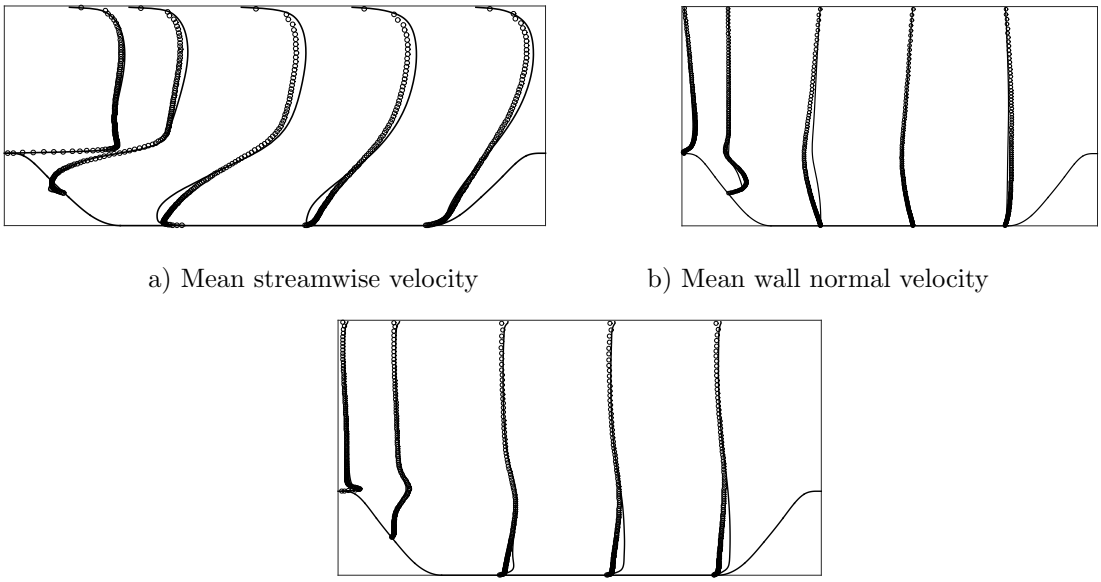

a) Mean streamwise velocity

b) Mean wall normal velocity

c) Mean streamwise velocity fluctuation

Figure 2: a) streamwise mean velocity b) wall normal mean velocity c) streamwise Reynolds stress over the periodic hill

4.2 Periodic Hill

The Reynolds number, $Re = 10595$ is based on the hill height h, the bulk velocity taken at the crest of the first hill, and the laminar viscosity. The domain dimensions are $9.0h \times 3.036h$, $h = 28mm$ and the flow is periodic in the streamwise direction. The mesh is $N_x \times N_y = 87 \times 85$. The cyclic boundary condition with

constant bulk velocity is applied at the inlet. The results are compared with the LES results of Frohlich et al. [8], see Fig. 2.

4.3 Asymmetric Diffuser

The configuration is an asymmetric plane diffuser, see Fig. 3, with a Reynolds number of $Re = U_{b,in}H/\nu = 18000$ ($H_{in} = 1$). The diffuser angle is 10°. The mesh is $N_x \times N_y = 2070 \times 80$. The homogeneous Neumann is applied for the turbulence quantities at the outlet boundary. The *inletOutlet* condition, which is the homogeneous Neumann condition with a limitation of no backflow, is applied at the outlet boundary for the velocity. The homogeneous Neumann condition is applied for the pressure at all boundaries. The results are compared with the experimental study of Buice and Eaton [10], see Fig. 3.

4.4 Dellenback abrupt expansion

The case studied in the present work is the swirling flow through a sudden 1:2 axisymmetric expansion that was experimentally examined by Dellenback et al. [12]. The origin is located on the centerline at the expansion. The inlet Reynolds number is 10^5, and the swirl number is 1.23. For more details about flow configuration and boundary conditions see Javadi and Nilsson ref. [11]. The mesh consists of 1.8×10^6 cells with 4.5×10^5 cells in the upstream of the expansion. Figure 4 shows the mean velocity and velocity fluctuation root mean square at $z/D = 0.25$ after expansion. The EBRSM model shows good agreement with experimental results. The main character of the flow, the vortex breakdown, is captured very well.

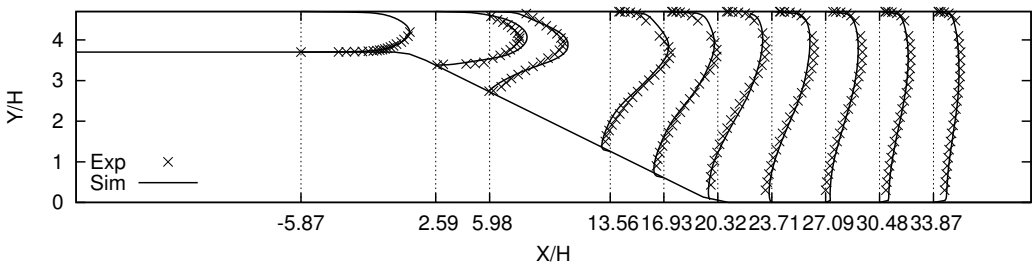

a) Mean streamwise velocity

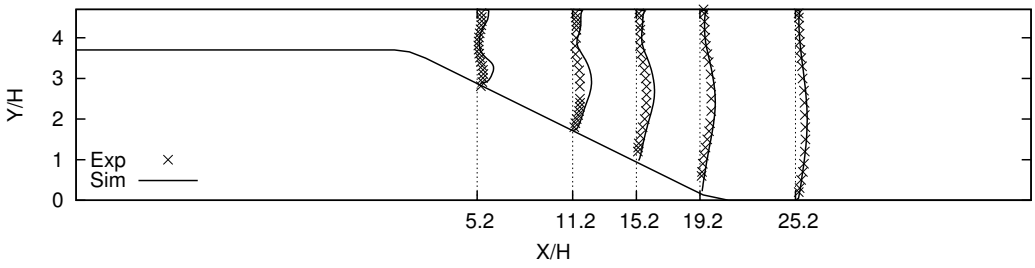

b) Mean streamwise velocity fluctuation

Figure 3: a) streamwise mean velocity b) Reynolds stresses in the asymmetric diffuser

References

[1] Durbin, P.A.: Near-wall turbulence closure modeling without 'damping functions'. Theor. Comput. Fluid Dyn. 3(1), (1991)

[2] Uzkan, T. and Reynolds, W. C.: A shear-free turbulent boundary layer. J . Fluid Mech. 28, 803-821 (1967)

[3] Thomas, N. H. and Hancock, P. E.: Grid turbulence near a moving wall. J . Fluid Mech. 82, 481-496 (1977)

[4] Rogers, M. M. and Moin, P.: The structure of the vorticity field in homogeneous turbulent flows. J . Fluid Mech. 176, 33-66 (1987)

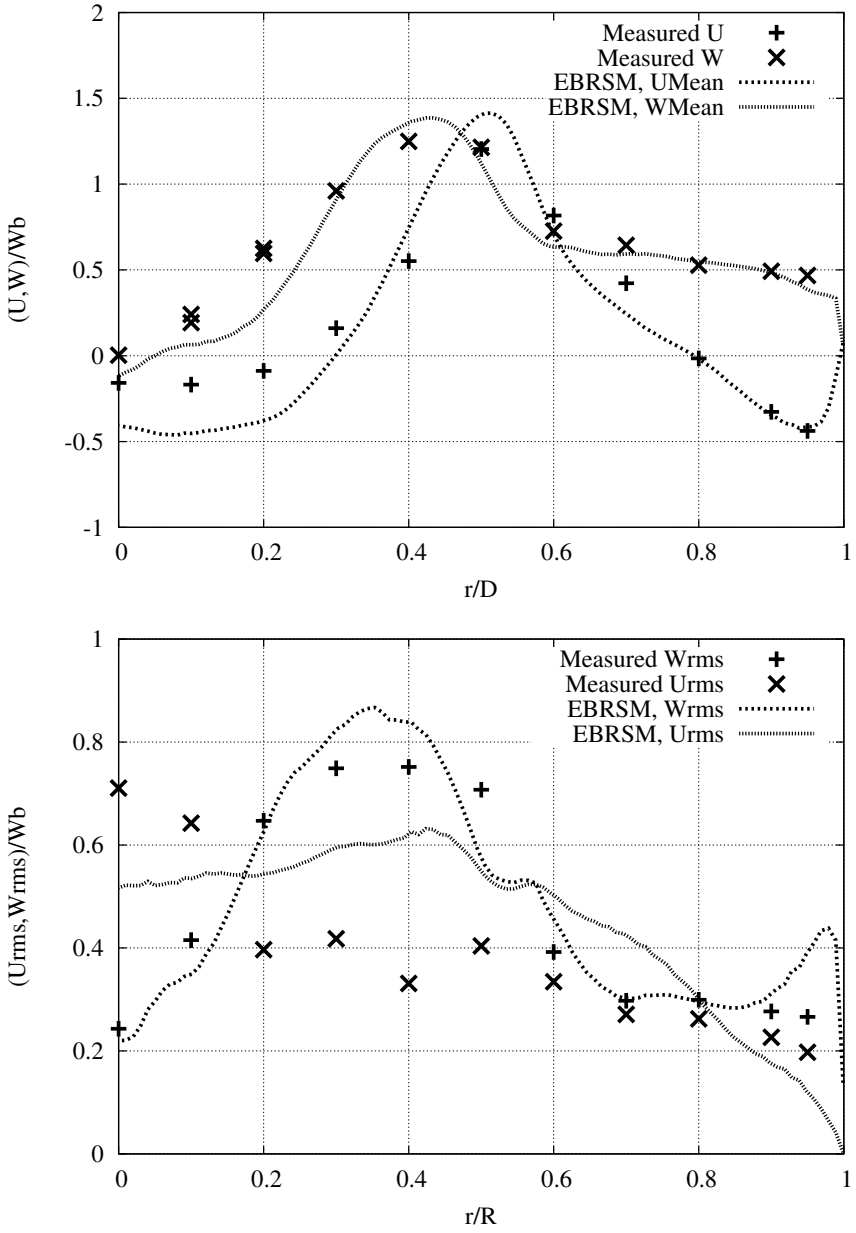

Figure 4: a) axial, *W*, and tangential, *U*, mean velocity normalized by bulk velocity at the inlet, b) axial, *Wrms*, and tangential, *Urms*, velocity fluctuation root mean square normalized by bulk velocity at the inlet,

[5] Hunt, J. C. R. and Graham, J. M. R.: Free-stream turbulence near plane boundaries. J . Fluid Mech. 84, 209-235 (1978)

[6] Moin, P. and Kim, J.: Numerical investigation of turbulent channel flow. J . Fluid Mech. 118, 341-377 (1982)

[7] Manceau, R. and Hanjalić , K.: Elliptic blending model: a new near-wall Reynolds stress turbulence closure. Phys. Fluids 14(2), 744–754 (2002)

[8] Frohlich, J., Mellen, C. P., Rodi, W., Temmerman, L., and Leschziner, M. A.: Highly resolved large-eddy simulation of separated flow in a channel with streamwise periodic constrictions. J. Fluid Mech. 526, 19-66 (2005)

[9] Moser, R.D., Kim, J. and Mansour, N.N.: Direct numerical simulation of turbulent channel flow up to Re= 590. Phys. Fluids, 11(4), 943-945 (1999)

[10] Buice, C.U. and Eaton, J.K.:Experimental Investigation of Flow Through an Asymmetric Plane Diffuser. J. Fluids Eng.122, 433-435 (2000)

[11] Javadi, A. and Nilsson, H.: LES and DES of strongly swirling turbulent flow through a suddenly expanding circular pipe. Comput. Fluids 107, 301-313 (2015)

[12] Dellenback, P. A., Metzger, D. E., Neitzel, G. P.: Measurements in turbulent swirling flow through an abrupt axisymmetric expansion. AIAA J. 26(6), 669–81 (1988)

[13] Schiestel, R. and Dejoan, A.: Towards a new partially integrated transport model for coarse grid and unsteady turbulent flow simulations. Theor. Comput. Fluid Dyn. 18, 443 (2005)

[14] Fadai-Ghotbi, A., Christophe F., Manceau, R. and J Borée, J.: A seamless hybrid RANS-LES model based on transport equations for the subgrid stresses and elliptic blending. Phys. Fluids, 22(5) (2010)